

Microchip laser operation of Yb-doped gallium garnets

Josep Maria Serres,¹ Venkatesan Jambunathan,² Pavel Loiko,^{1,3} Xavier Mateos,^{1,4,7,*}
Haohai Yu,⁵ Huaijin Zhang,⁵ Junhai Liu,⁶ Antonio Lucianetti,² Tomas Mocek,²
Konstantin Yumashev,³ Uwe Griebner,⁴ Valentin Petrov,⁴ Magdalena Aguiló,¹ and
Francesc Díaz¹

¹Física i Cristal·lografia de Materials i Nanomaterials (FiCMA-FiCNA), Universitat Rovira i Virgili (URV), Campus Sescelades, c/ Marcel·lí Domingo, s/n., Tarragona, E-43007, Spain

²HiLASE Centre, Institute of Physics CAS, Za Radnicí 828, Dolní Břežany, 25241, Czech Republic

³Center for Optical Materials and Technologies, Belarusian National Technical University, 65/17 Nezavisimosti Ave., Minsk, 220013, Belarus

⁴Max Born Institute for Nonlinear Optics and Short Pulse Spectroscopy, Max-Born-Str. 2a, Berlin, D-12489, Germany

⁵State Key Laboratory of Crystal Materials, Shandong University, Jinan, 250100, China

⁶College of Physics, Qingdao University, 308 Ning-Xia Road, Qingdao, 266071, China

⁷xavier.mateos@urv.cat

*mateos@mbi-berlin.de

Abstract: Continuous-wave microchip laser operation and thermal lensing are studied for Yb-doped gallium garnets, Yb:LuGG, Yb:YGG, Yb:CNGG and Yb:CLNGG under diode-pumping at ~932 and 969 nm. It is shown that although thermal the conductivity of Ga garnets is lower than that of Yb:YAG, the compromised thermo-optic properties, high absorption in the zero-phonon line and low internal loss make the ordered Yb:YGG and Yb:LuGG crystals to be promising for compact highly efficient microchip lasers. In particular, Yb:LuGG microchip laser generated 8.97 W of output power with a slope efficiency $\eta = 75\%$ and 9.31 W with $\eta = 65\%$, for pumping at 932 and 969 nm, respectively. Multi-watt output in the range 1039–1078 nm is emitted for different transmission of the output coupler. The sensitivity factor of the thermal lens for this crystal is $2.1 \text{ m}^{-1}/\text{W}$ (pumping at 969 nm with a pump waist radius of 100 μm) and the estimated thermal conductivity is $5.8 \pm 0.5 \text{ W/mK}$. Power scaling of Yb:CNGG and Yb:CLNGG microchip lasers is limited by poor thermo-optic properties and high internal losses. Ordered Ga garnets show good prospects for the development of passively Q-switched microchip lasers with high pulse energies.

©2015 Optical Society of America

OCIS codes: (140.3380) Laser materials; (140.6810) Thermal effects; (140.3480) Lasers, diode-pumped.

References and links

1. S. Chénais, F. Druon, F. Balembois, P. Georges, A. Brenier, and G. Boulon, “Diode-pumped Yb:GGG laser: Comparison with Yb:YAG,” *Opt. Mater.* **22**(2), 99–106 (2003).
2. R. L. Aggarwal, D. J. Ripin, J. R. Ochoa, and T. Y. Fan, “Measurement of thermo-optic properties of $\text{Y}_3\text{Al}_5\text{O}_{12}$, $\text{Lu}_3\text{Al}_5\text{O}_{12}$, YAlO_3 , LiYF_4 , LiLuF_4 , BaY_2F_8 , $\text{KGd}(\text{WO}_4)_2$, and $\text{KY}(\text{WO}_4)_2$ laser crystals in the 80–300 K temperature range,” *J. Appl. Phys.* **98**, 103514 (2005).
3. Y. Sato and T. Taira, “The studies of thermal conductivity in GdVO_4 , YVO_4 , and $\text{Y}_3\text{Al}_5\text{O}_{12}$ measured by quasi-one-dimensional flash method,” *Opt. Express* **14**(22), 10528–10536 (2006).
4. Y. Sato, J. Akiyama, and T. Taira, “Effects of rare-earth doping on thermal conductivity in $\text{Y}_3\text{Al}_5\text{O}_{12}$ crystals,” *Opt. Mater.* **31**(5), 720–724 (2009).
5. J. Saikawa, S. Kurimura, I. Shoji, and T. Taira, “Tunable frequency-doubled Yb:YAG microchip lasers,” *Opt. Mater.* **19**(1), 169–174 (2002).
6. W. Han, K. Wu, X. Tian, L. Xia, H. Zhang, and J. Liu, “Laser performance of ytterbium-doped gallium garnets: Yb:Re₃Ga₅O₁₂ (Re = Y, Gd, Lu),” *Opt. Mater. Express* **3**(7), 920–927 (2013).

7. H. Yu, K. Wu, B. Yao, H. Zhang, Z. Wang, J. Wang, Y. Zhang, Z. Wei, Z. Zhang, X. Zhang, and M. Jiang, "Growth and characteristics of Yb-doped $\text{Y}_3\text{Ga}_5\text{O}_{12}$ laser crystal," *IEEE J. Quantum Electron.* **46**(12), 1689–1695 (2010).
8. K. Wu, L. Hao, H. Zhang, H. Yu, Y. Wang, J. Wang, X. Tian, Z. Zhou, J. Liu, and R. I. Boughton, " $\text{Lu}_3\text{Ga}_5\text{O}_{12}$ crystal: exploration of new laser host material for the ytterbium ion," *J. Opt. Soc. Am. B* **29**(9), 2320–2328 (2012).
9. X. Zhang, A. Brenier, Q. Wang, Z. Wang, J. Chang, P. Li, S. Zhang, S. Ding, and S. Li, "Passive Q-switching characteristics of $\text{Yb}^{3+}:\text{Gd}_3\text{Ga}_5\text{O}_{12}$ crystal," *Opt. Express* **13**(19), 7708–7719 (2005).
10. Y. Zhang, Z. Wei, Q. Wang, D. Li, Z. Zhang, H. Yu, H. Zhang, J. Wang, and L. Lv, "Diode-pumped efficient continuous-wave Yb: $\text{Y}_3\text{Ga}_5\text{O}_{12}$ laser at 1035 nm," *Opt. Lett.* **36**(4), 472–474 (2011).
11. Y. Zhang, Z. Wei, B. Zhou, C. Xu, Y. Zou, D. Li, Z. Zhang, H. Zhang, J. Wang, H. Yu, K. Wu, B. Yao, and J. Wang, "Diode-pumped passively mode-locked Yb: $\text{Y}_3\text{Ga}_5\text{O}_{12}$ laser," *Opt. Lett.* **34**(21), 3316–3318 (2009).
12. Yu. K. Voronko, A. A. Sobol, A. Ya. Karasik, N. A. Eskov, P. A. Rabochkina, and S. N. Ushakov, "Calcium niobium gallium and calcium lithium niobium gallium garnets doped with rare earth ions – effective laser media," *Opt. Mater.* **20**(3), 197–209 (2002).
13. H. Zhang, J. Liu, J. Wang, J. Fan, X. Tao, X. Mateos, V. Petrov, and M. Jiang, "Spectroscopic properties and continuous-wave laser operation of a new disordered crystal: Yb-doped CNGG," *Opt. Express* **15**(15), 9464–9469 (2007).
14. V. Lupei, A. Lupei, C. Gheorghe, L. Gheorghe, A. Achim, and A. Ikesue, "Crystal field disorder effects in the optical spectra of Nd^{3+} and Yb^{3+} -doped calcium lithium niobium gallium garnets laser crystals and ceramics," *J. Appl. Phys.* **112**(6), 063110 (2012).
15. A. Lupei, V. Lupei, L. Gheorghe, L. Rogobete, E. Osiac, and A. Petraru, "The nature of nonequivalent Nd^{3+} centers in CNGG and CLNGG," *Opt. Mater.* **16**(3), 403–411 (2001).
16. J. H. Liu, Y. Wan, Z. Zhou, X. Tian, W. Han, and H. Zhang, "Comparative study on the laser performance of two Yb-doped disordered garnet crystals: Yb:CNGG and Yb:CLNGG," *Appl. Phys. B* **109**(2), 183–188 (2012).
17. J. Liu, W. Kong, X. Tian, Zh. Zhou, W. Han, Sh. Han, and H. Zhang, "Efficient laser oscillation of a new disordered Yb:CLNGG crystal," *Laser Phys. Lett.* **9**(5), 394–397 (2012).
18. Y. Zhang, V. Petrov, U. Griebner, X. Zhang, S. Y. Choi, J. Y. Gwak, F. Rotermund, X. Mateos, H. Yu, H. Zhang, and J. Liu, "90-fs diode-pumped Yb:CLNGG laser mode-locked using single-walled carbon nanotube saturable absorber," *Opt. Express* **22**(5), 5635–5640 (2014).
19. A. Schmidt, U. Griebner, H. Zhang, J. Wang, M. Jiang, J. Liu, and V. Petrov, "Passive mode-locking of the Yb:CNGG laser," *Opt. Commun.* **283**(4), 567–569 (2010).
20. J. J. Zayhowski, "Microchip lasers," *Opt. Mater.* **11**(2-3), 255–267 (1999).
21. J. M. Serres, P. Loiko, X. Mateos, K. Yumashev, N. Kuleshov, V. Petrov, U. Griebner, M. Aguiló, and F. Díaz, "Prospects of monoclinic Yb:KLu(WO_4)₂ crystal for multi-watt microchip lasers," *Opt. Mater. Express* **5**(3), 661–667 (2015).
22. S. Chénais, F. Druon, S. Forget, F. Balembois, and P. Georges, "On thermal effects in solid-state lasers: The case of ytterbium-doped materials," *Prog. Quantum Electron.* **30**(4), 89–153 (2006).
23. Y. Sato and T. Taira, "Highly accurate interferometric evaluation of thermal expansion and dn/dT of optical materials," *Opt. Mater. Express* **4**(5), 876–888 (2014).
24. T. Taira, J. Saikawa, T. Kobayashi, and R. L. Byer, "Diode-pumped tunable Yb:YAG miniature lasers at room temperature: modeling and experiment," *IEEE J. Sel. Top. Quantum Electron.* **3**(1), 100–104 (1997).
25. J. Dong, A. Shirakawa, K.-I. Ueda, and A. A. Kaminskii, "Effect of ytterbium concentration on cw Yb:YAG microchip laser performance at ambient temperature – Part I: Experiments," *Appl. Phys. B* **89**(2-3), 359–365 (2007).
26. P. A. Loiko, J. M. Serres, X. Mateos, K. V. Yumashev, N. V. Kuleshov, V. Petrov, U. Griebner, M. Aguiló, and F. Díaz, "Thermal lensing in Yb:KLu(WO_4)₂ crystals cut along the optical indicatrix axes," *Laser Phys. Lett.* **11**(12), 125802 (2014).
27. P. Loiko, F. Druon, P. Georges, B. Viana, and K. Yumashev, "Thermo-optic characterization of Yb:CaGdAlO₄ laser crystal," *Opt. Mater. Express* **4**(11), 2241–2249 (2014).
28. M. J. Weber, *Handbook of optical materials* (CRC Press, New York, 2003).
29. J. A. Caird, S. A. Payne, P. R. Staber, A. J. Ramponi, L. L. Chase, and W. F. Krupke, "Quantum electronic properties of the $\text{Na}_3\text{Ga}_2\text{Li}_3\text{F}_{12}:\text{Cr}^{3+}$ laser," *IEEE J. Quantum Electron.* **24**(6), 1077–1099 (1988).
30. J. Dong, M. Bass, Y. Mao, P. Deng, and F. Gan, "Dependence of the Yb^{3+} emission cross section and lifetime on temperature and concentration in yttrium aluminum garnet," *J. Opt. Soc. Am. B* **20**(9), 1975–1979 (2003).
31. J. Dong, K. Ueda, A. Shirakawa, H. Yagi, T. Yanagitani, and A. A. Kaminskii, "Composite Yb:YAG/ Cr^{4+} :YAG ceramics picosecond microchip lasers," *Opt. Express* **15**(22), 14516–14523 (2007).

1. Introduction

Ytterbium (Yb^{3+}) ions are attractive for high-power, efficient and wavelength-tunable laser operation near 1 μm related to their single ${}^2\text{F}_{5/2} \rightarrow {}^2\text{F}_{7/2}$ transition. Yb lasers enable power scaling due to a low quantum defect (Stokes shift) between the pump λ_p and laser λ_l wavelengths and because they can be pumped with commercially available, high-power InGaAs laser diodes emitting at 930–980 nm. The Yb^{3+} ion is also free of unwanted parasitic

processes such as excited-state absorption and up-conversion and it typically shows very high luminescence quantum yield leading to exceptionally high laser efficiency (> 80%).

The traditional host for Yb³⁺ doping is the cubic yttrium aluminium garnet, Y₃Al₅O₁₂ (YAG). It possesses good thermo-optical and thermo-mechanical properties as well as relatively high thermal conductivity κ . However, Yb:YAG show a pronounced drop of κ with the Yb concentration. A high Yb concentration is required to achieve high pump efficiency (high absorption) which is advantageous for the development of compact laser sources [1]. In particular, κ is ~10 W/mK for undoped YAG and it drops to ~7 W/mK for only 5 at.% Yb doping [2,3]. Moreover, heating of YAG to about 100 °C (value taken as an estimate of the typical temperature rise in diode pumped systems) would lead to a further drop to ~6 W/mK [4]. The emission band for Yb:YAG is narrower than that of low-symmetry disordered Yb materials. Thus, although the possible tuning range for Yb:YAG is relatively broad (1024 – 1108 nm as achieved with a very high reflectivity of the cavity mirrors [5]), one can expect broader tuning possibilities with disordered garnets also accessible with less strict requirements to the cavity mirrors. Thus, the search of new materials for Yb³⁺ doping within the garnet family, A₃B₂C₃O₁₂ (where A = Ca, La, Y, Gd or Lu, B = Al, Ga, Fe, Sc and C = Al, Fe, Ge, or Ga) is ongoing. In particular, gallium garnets attracted a lot of attention during the recent years.

In the present work, we compare two groups of gallium garnets. The first one comprises ordered crystals with chemical formula RE₃Ga₅O₁₂ (REGG) where RE = Gd, Y or Lu [6]. They are usually grown by the optical floating zone method [7]. Large-volume and highly-doped (10 at.% Yb) crystals with good optical homogeneity can be obtained. The thermal conductivity of ~7 at.% doped Yb:REGG is ~5 W/mK and their physical properties are in general similar to those of YAG [8]. The spectroscopic properties of Yb³⁺ ions in REGG were previously studied [7,8]. Continuous-wave (CW), Q-switched and mode-locked operation with Yb:REGG crystals was also reported [9–11]. A CW Yb:YGG laser generated 6.75 W at ~1070 nm with a slope efficiency η of 80% [6].

The second group includes cubic crystals with intrinsic disorder, like calcium niobium gallium garnet. Its stoichiometric composition is Ca₃(Nb_{1.5}Ga_{0.5})Ga₃O₁₂ (shortly CNGG). This crystal can be grown by the Czochralski method using platinum crucibles as it melts at 1773 K (temperature lower than for YAG, 2223 K) [12]. More exactly, Ca₃Nb_{1.5 + 1.5x}Ga_{3.5 - 2.5x}□_xO₁₂ compounds (where □ is a cationic vacancy) melt congruently. However, the presence of cationic vacancies is unwanted for high power laser operation. Incorporation of Li⁺ can eliminate these vacancies forming a new crystal, Ca₃Li_yNb_{1.5 + y}Ga_{3.5 - 2y}O₁₂ (shortly CLNGG) [13]. Yb:CNGG and Yb:CLNGG crystals possess still reasonable thermal conductivity, ~3.5 W/mK [11] and their emission bands are broader than that of Yb:YAG [14]. This is due to the above mentioned intrinsic disorder for these crystals, as Nb⁵⁺ and Ga³⁺ ions randomly occupy the same octahedral *a*-sites with six-O²⁻ coordination and C_{3i} local symmetry [15]. Laser experiments with Yb:CNGG and Yb:CLNGG crystals proved the potential of the latter for power scaling [16]. In [17], the Yb:CLNGG laser generated 5 W of CW output power at 1038 nm with η = 83%. Pulsed laser operation with these crystals was also reported [18,19].

In a microchip laser the active medium is placed in a compact plano-plano cavity providing low loss, high efficiency and robust design [20]. The key point for the stabilization of the laser mode in the microchip laser is the positive thermal lens (thermal mechanism) [21]. It can be expected to be positive for all cubic garnets [22] because they possess positive thermo-optic coefficients (dn/dT ~8 × 10⁻⁶ K⁻¹ [23]). In addition, a low anisotropy of the elastic properties inherent to the cubic structure will correspond to a low astigmatism of the lens and, hence, to excellent quality of the laser beam [22].

In the present work, we compare the thermal lensing and microchip laser performance of a series of Yb-doped gallium garnets with ordered, Yb:YGG and Yb:LuGG, as well as disordered, Yb:CNGG and Yb:CLNGG, crystal structure. This study was also motivated by high slope efficiencies and output powers achieved previously in longitudinally diode pumped Yb:YAG microchip lasers [5,24,25].

2. Experimental

We studied four Yb-doped gallium garnets, Yb:LuGG and Yb:YGG (grown in an oxygen atmosphere by the optical floating zone method), and Yb:CNGG and Yb:CLNGG (grown by the Czochralski method). From the as-grown bulks, rectangular samples were cut along the [111] crystallographic direction. Their thickness, aperture and doping level are specified in Table 1. The samples were polished to laser quality and remained uncoated. They were wrapped with indium foil to improve the thermal contact and mounted in a water-cooled copper holder kept at $\sim 12^\circ\text{C}$.

Table 1. Compositional and Geometrical Parameters of the Studied Laser Crystals

Crystal	Growth method	Doping, at.%	N_{Yb} , 10^{20} cm^{-3}	Thickness, mm	Aperture, mm^2
Yb:LuGG	optical floating zone	7.13	9.4	6.00	3×3
Yb:YGG	optical floating zone	7.35	9.7	6.02	3×3
Yb:CNGG	Czochralski	5.80	7.1	8.00	5×5
Yb:CLNGG	Czochralski	4.30	5.3	3.14	3×3

The microchip laser cavity consisted of a flat pump mirror (PM), AR coated for $0.9\text{--}1.0\ \mu\text{m}$ and HR coated for $1.02\text{--}1.20\ \mu\text{m}$, and a set of flat output couplers (OC) with transmission $T_{\text{OC}} = 1\%$, 5% or 10% at the laser wavelength. The cavities contained no air gaps so that their lengths were equal to the geometrical length of the crystals. Two fiber-coupled InGaAs diodes were used, nominally emitting at around $\sim 932\ \text{nm}$ and $969\ \text{nm}$. The pump beam was focused into the crystals with a lens assembly having a reimaging ratio of 1:1 and a focal length of $30\ \text{mm}$. The first diode (#1), emitting at $932\ \text{nm}$, had a fiber core diameter of $105\ \mu\text{m}$ and N.A. of 0.14 . The second diode (#2) was stabilized by a Volume Bragg Grating (VBG) and emitted at $969\ \text{nm}$. Its fiber core diameter was $200\ \mu\text{m}$ and N.A. = 0.22 . Both diodes provided a maximum output power of $25\ \text{W}$. The pump spot sizes in the focus w_p and confocal parameters $2z_R$ were then $\sim 52\ \mu\text{m}/1.0\ \text{mm}$ and $100\ \mu\text{m}/3.2\ \text{mm}$, respectively. The crystals were pumped in a single-pass configuration.

Typical emission spectra for the used diodes are shown in Fig. 1. Diode #1 provided multi-peak emission with a full width at half maximum (FWHM) of $\sim 5.5\ \text{nm}$. With the increase of the diode current, the central emission wavelength shifted from $927\ \text{nm}$ to $935\ \text{nm}$. The emission of diode #2 had a FWHM of $\sim 0.3\ \text{nm}$ and the central wavelength was $969.5 \pm 0.1\ \text{nm}$.

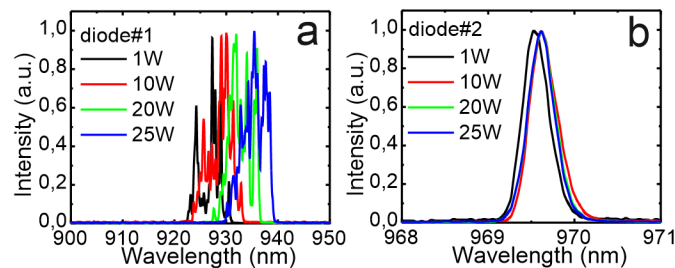


Fig. 1. Emission spectra of the employed laser diodes for various values of their output power.

The measured absorption of the pump light in the studied crystals vs. the incident pump power for both diodes is shown in Fig. 2. The observed dependences are attributed to the depletion of the pump absorption (for both diodes) and the temperature drift of the diode emission wavelength in the case of diode #1, see Fig. 1. The pump saturation intensity for the studied crystals was estimated to be $\sim 20\ \text{kW}/\text{cm}^2$. For Yb:LuGG, Yb:YGG and Yb:CNGG the pump absorption at high pump level was $60\text{--}70\%$ while for Yb:CLNGG it was $\sim 50\%$ due to the shorter length of the crystal.

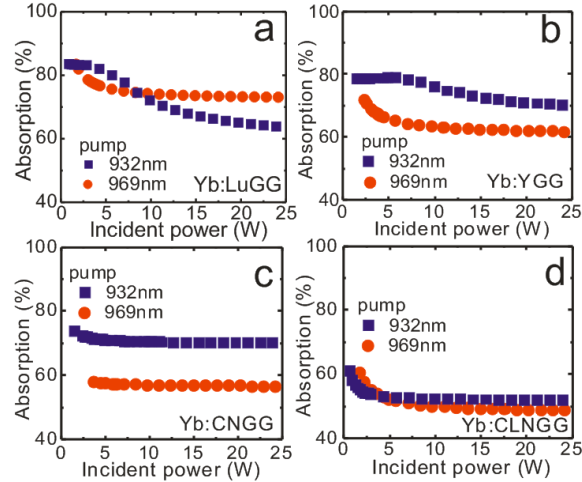


Fig. 2. Absorption in the Yb:LuGG (a), Yb:YGG (b), Yb:CNGG (c), and Yb:CLNGG (d) crystals vs. incident pump power for the two pump diodes employed.

The pump sources operating at the above mentioned wavelengths were selected with respect to the absorption cross-section (σ_{abs}) curves of the Yb-doped gallium garnets, see Fig. 3(a). At room-temperature (293 K), the zero-phonon line for Yb:YGG and Yb:LuGG crystals is centered at 970.4 nm (FWHM ~ 1.8 nm), for Yb:CNGG at 973.5 nm (FWHM = 4.4 nm) and for Yb:CLNGG at 971.6 nm (FWHM = 3.5 nm). The broader zero-phonon line for Yb:CNGG and Yb:CLNGG crystals is related to the above mentioned intrinsic disorder. The emission of the VBG-stabilized diode #2 corresponds to this line. Although its emission does not precisely match the absorption peak, the absorption cross-section amounts to $\sigma_{\text{abs}} \sim 1...2 \times 10^{-20} \text{ cm}^2$. The absorption spectra between 918 and 945 nm are characterized by a wide plateau, Fig. 3(a). It corresponds to the same average value of σ_{abs} . Diode #1 emitting at around 932 nm is applied for pumping in the plateau range because it is less sensitive to the wavelength-dependent temperature drift of the diode.

In Fig. 3(b), the stimulated-emission cross-section σ_{SE} spectra for the studied crystals are shown. The peak σ_{SE} values are slightly higher for Yb:YGG and Yb:LuGG ($\sim 2.6 \times 10^{-20} \text{ cm}^2$) but Yb:CNGG and Yb:CLNGG provide broader emission bands (FWHM ~ 24 nm).

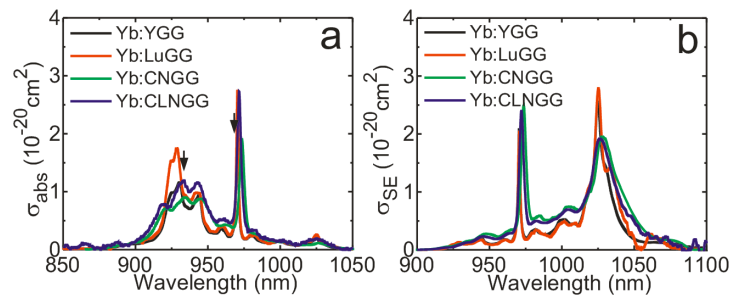


Fig. 3. Absorption (a) and stimulated-emission (b) cross-section spectra of the studied Yb-doped gallium garnets.

To study the thermal lensing, the crystals were placed in a hemispherical cavity. The PM was the same and the OC was concave ($R = 50$ mm) having $T_{\text{OC}} = 3\%$ with a total cavity length of 49 mm. The laser diode emitting at 969 nm was used to pump the crystals. Optical (refractive) power of the thermal lens was evaluated from the divergence of the output beam using the ABCD formalism, the details can be found elsewhere [26].

3. Results and discussion

The results on thermal lens measurements are shown in Fig. 4. Here the optical power of the thermal lens D is plotted vs. the absorbed pump power P_{abs} . The slope of this dependence defines the so-called sensitivity factor, $M = dD/dP_{\text{abs}}$ [27]. For all studied crystals, laser operation in the hemispherical cavity was achieved at $\sim 1048 \pm 1$ nm. The Stokes shift between the pump and laser wavelength, $1 - \lambda_p/\lambda_l$, was 7.5%. Without polarizing elements in the cavity, the laser emission was partially polarized (polarization degree: $>60\%$). Partially polarized emission is typical for cubic and optically isotropic garnets and it is attributed to the losses induced by the thermal lens. The value of D was determined then for the directions parallel and orthogonal to the laser polarization as they should correspond to the principal meridional planes of the thermal lens usually denoted as “r” and “ θ ”, respectively [22]. In Fig. 4, the D_r values are shown. As expected, the values of D_r are larger than D_θ . The difference of the D -values, denoted as astigmatism degree [27], amounted to $\sim 15 \pm 5\%$. This agrees well with the theoretical predictions for Yb:YAG [22].

The sensitivity factors of the thermal lens are similar for Yb:YGG and Yb:LuGG, $M = 2.0$ and $2.1 \text{ m}^{-1}/\text{W}$, respectively. These values are close to those reported previously for Yb:GGG crystal (pumping at $971 \text{ nm} / w_p = 120 \text{ }\mu\text{m}$), $M = 2.26 \text{ m}^{-1}/\text{W}$ [1]. For Yb:CLNGG, the thermal lens is stronger, $M = 3.9 \text{ m}^{-1}/\text{W}$ and for Yb:CNGG, the value of M is the highest, $5.0 \text{ m}^{-1}/\text{W}$. This difference is attributed mainly to the difference of thermal conductivity κ for the studied crystals. The M -factor of the thermal lens for a diode-pumped crystal is [22]:

$$M_{r,\theta} = \frac{\eta_h}{2\pi w_p^2 \kappa} \chi_{r,\theta} \quad (1)$$

Here, w_p is the “average” radius of the pump beam in the crystal since the confocal parameter for the pump beam $2z_R$ is shorter than the crystal length. η_h is the fractional heat loading which is estimated as Stokes shift, and $\chi_{r,\theta}$ is the “generalized” thermo-optic coefficient. It was shown in [22] that for all cubic garnets, the values of $\chi_{r,\theta}$ are very close to those of YAG, $\chi_r = 16.6$ and $\chi_\theta = 15.4 \times 10^{-6} \text{ K}^{-1}$, due to the similar thermal and elastic properties [28]. The latter allows one to estimate the thermal conductivity κ of the studied crystals using Eq. (1).

For Yb:LuGG and Yb:YGG crystals, κ is estimated to be $5.8 \pm 0.5 \text{ W/mK}$, and for Yb:CLNGG and Yb:CNGG crystals, $\kappa = 3.2$ and $2.5 \pm 0.5 \text{ W/mK}$, respectively. These values correspond to the optically pumped (and thus heated) crystals. They are in agreement with previous reports [8,11].

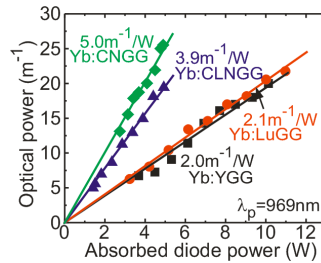


Fig. 4. Optical power of the thermal lens vs. absorbed power at 969 nm for Yb-doped gallium garnets: *symbols* are the experimental data, *lines* are for the calculation of the sensitivity factor. The laser wavelength is ~ 1048 nm.

It should be noted that determined parameters of the thermal lens are independent on the configuration of the laser cavity and are characteristic only for the used pump configuration (in particular, the pump spot radius w_p). In accordance with Eq. (1), M -factors are inversely proportional to the square of w_p , so $M' = M(w_p/w_p')^2$. The measured parameters of the thermal lens allowed us to estimate radii of the laser mode for microchip laser cavities with the studied crystals, $w_l = 60 \pm 10 \text{ }\mu\text{m}$ (969 nm pumping) and $45 \pm 5 \text{ }\mu\text{m}$ (932 nm pumping).

Taking into account the different pump spot sizes in the focus w_p and confocal parameters $2z_R$ for the used diodes, this leads to a close overlap integrals for pump and laser modes in the microchip cavity, $\sim 0.6 \pm 0.1$ for both pump diodes.

Microchip laser operation was achieved with all garnets using the two described pump diodes. The input-output dependences for these lasers pumped at ~ 932 nm are shown in Fig. 5 with respect to the absorbed power. The Yb:LuGG crystal demonstrated superior laser performance. For $T_{OC} = 10\%$, a maximum output power of 8.97 W was achieved at 1040 nm with a slope efficiency $\eta = 75\%$. The optical-to-optical efficiency was 63% and the laser threshold was at $P_{abs} = 1.22$ W. Using OCs with 5% and 1% transmission, the slope efficiency dropped to 69% and 62%, respectively.

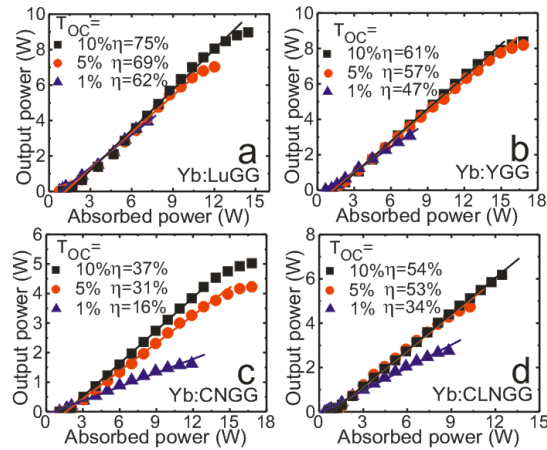


Fig. 5. Input-output dependences for microchip lasers based on Yb:LuGG (a), Yb:YGG (b), Yb:CNGG (c) and Yb:CLNGG (d) crystals. The pump wavelength is ~ 932 nm, η - slope efficiency.

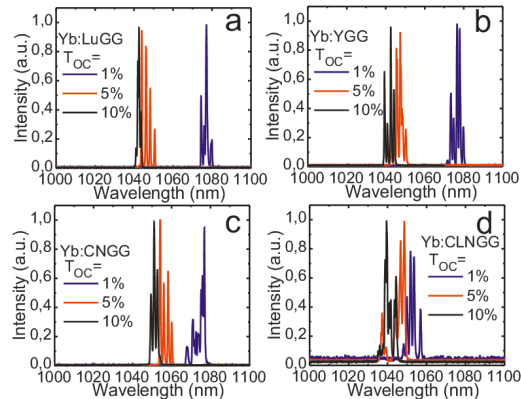


Fig. 6. Microchip laser emission spectra for Yb:LuGG (a), Yb:YGG (b), Yb:CNGG (c) and Yb:CLNGG (d) diode-pumped at 932 nm. The absorbed power is 7 W.

The Yb:YGG crystal showed slightly inferior laser performance. The maximum output power was 8.40 W at 1042 nm with $\eta = 61\%$ for $T_{OC} = 10\%$. For Yb:CNGG and Yb:CLNGG microchip lasers, substantially lower output power was achieved. This decrease is attributed to the stronger thermo-optic effects in these crystals, Fig. 4. The maximum output power generated with Yb:CLNGG was 6.1 W at 1039 nm with $\eta = 54\%$ and with Yb:CNGG it was 5.1 W at 1051 nm with $\eta = 37\%$ (both for $T_{OC} = 10\%$).

For all crystals, thermal roll-over in the output dependences is observed. The range of P_{abs} corresponding to a linear input-output curve narrows at lower T_{OC} . For Yb:LuGG, Fig. 5(a), thermal roll-over starts at $P_{\text{abs}} \sim 7, 11$ and 13 W for $T_{\text{OC}} = 1\%, 5\%$ and 10% , respectively.

Typical laser emission spectra for all microchip lasers are shown in Fig. 6. All of them show a multi-peak behavior. For Yb:YGG and Yb:LuGG, the use of $T_{\text{OC}} = 1\%$ corresponded to laser oscillation at ~ 1080 nm and with 5% and 10% OCs, laser emission occurred at ~ 1050 and 1040 nm, respectively. For Yb:CNGG and Yb:CLNGG, the shift of the emission wavelength was less pronounced. In the latter case, λ_l was $\sim 1052, 1048$ and 1039 nm for $T_{\text{OC}} = 10\%, 5\%$ and 1% , respectively.

The recorded laser emission spectra help to explain the peculiarities of the thermal roll-over in the output dependences of the studied microchip lasers. The reason is a relatively high heat load under 932 nm pumping, as well as strongly localized heat deposition (as w_p was only ~ 52 μm). In particular, for Yb:LuGG laser, the value of η_h estimated as Stokes shift, was $13.2\%, 10.9\%$ and 10.2% for $1\%, 5\%$ and 10% OC, respectively. Thus, stronger heat load is expected for lower T_{OC} , leading to a thermal roll-over at lower P_{abs} , as seen in Fig. 5.

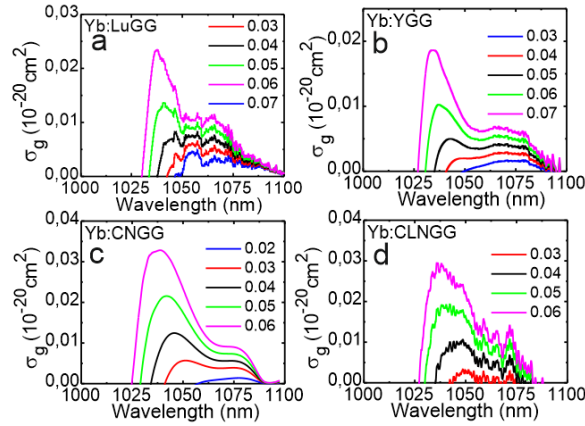


Fig. 7. Calculated gain cross-sections of Yb:LuGG (a), Yb:YGG (b), Yb:CNGG (c) and Yb:CLNGG (d) crystals for different inversion ratios β .

The observed blue-shift of the laser wavelength with the increase of T_{OC} is typical for quasi-three-level Yb lasers and is explained with the gain cross-section, σ_g , spectra, Fig. 7. Here, $\sigma_g = \beta\sigma_{\text{SE}} - (1-\beta)\sigma_{\text{abs}}$ where β is the inversion ratio, $\beta = N_2/N_0$ where N_2 and N_0 are the number of ions excited in the upper laser level and overall number of ions, respectively. The gain spectra of Yb:LuGG, Yb:YGG and Yb:CNGG at very low β , typical for CW microchip lasers, are flat and very broad in the range from ~ 1060 to 1080 nm. For Yb:CLNGG, this range extends from 1040 to 1080 nm. With the increase of β , an absolute maximum is formed in the gain spectra and its position is shifting from 1045 to 1030 nm. These spectral features are in good agreement with the recorded laser emission spectra, Fig. 6.

The output characteristics of the microchip lasers pumped at ~ 932 nm are summarized in Table 2.

Table 2. Output Characteristics of the Microchip Lasers Based on Gallium Garnets Pumped at 932 nm

Crystal	T_{OC} , %	P_{th} , W	P_{out} , W	η , %	Crystal	T_{OC} , %	P_{th} , W	P_{out} , W	η , %
Yb:LuGG	1	0.74	3.95	62	Yb:CNGG	1	1.06	1.60	16
	5	0.91	7.02	69		5	1.63	4.13	31
	10	1.22	8.97	75		10	1.75	5.05	37
Yb:YGG	1	0.76	3.02	47	Yb:CLNGG	1	0.47	2.75	34
	5	1.13	8.19	57		5	0.67	4.73	53
	10	1.34	8.40	61		10	0.82	6.18	54

The output characteristics of the microchip lasers pumped at 969 nm are collected in Fig. 8. Pumping with this diode provided a lower quantum defect ($\eta_h \sim 6\text{--}8\%$, depending on the OC) so that the input-output dependences remained linear in the entire pump range studied, up to at least 16 W of P_{abs} (for Yb:REGG) or 12 W (for Yb:CNGG and Yb:CLNGG). The maximum slope efficiency ($\eta = 71\%$) was achieved with Yb:YGG using $T_{\text{OC}} = 10\%$ with a maximum output power of 8.68 W at 1044 nm. The optical-to-optical efficiency was 58% and the threshold was at $P_{\text{abs}} = 2.52$ W due to the larger pump spot size ($w_p = 100 \mu\text{m}$).

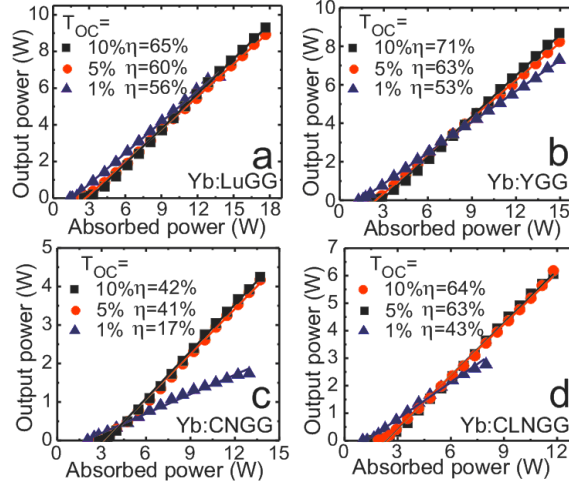


Fig. 8. Input-output dependences for microchip lasers based on Yb:LuGG (a), Yb:YGG (b), Yb:CNGG (c) and Yb:CLNGG (d). The pump wavelength is 969 nm, η - slope efficiency.

The Yb:LuGG laser showed slightly inferior performance, with maximum $\eta = 65\%$. However, with this crystal we extracted the maximum output power, 9.31 W at 1045 nm (using $T_{\text{OC}} = 10\%$). For both Yb:CNGG and Yb:CLNGG lasers, pumping at 969 nm improved the slope efficiency ($\eta = 42\%$ and 64% , respectively) with respect to the 932 nm pump while the level of the output power remained nearly the same (4.25 W and 6.18 W, respectively, for $T_{\text{OC}} = 10\%$). A summary of the laser characteristics for 969 nm pumping is presented in Table 3. The laser emission spectra for this pump wavelength were very similar to those presented in Fig. 6 for 932 nm pumping.

Table 3. Output Characteristics of the Microchip Lasers Based on Gallium Garnets Pumped at 969 nm

Crystal	T_{OC} , %	P_{th} , W	P_{out} , W	η , %	Crystal	T_{OC} , %	P_{th} , W	P_{out} , W	η , %
Yb:LuGG	1	1.63	6.62	56	Yb:CNGG	1	2.05	1.74	17
	5	2.40	8.93	60		5	2.80	4.17	41
	10	2.77	9.31	65		10	3.29	4.25	42
Yb:YGG	1	1.37	7.29	53	Yb:CLNGG	1	1.42	2.95	43
	5	2.32	8.24	63		5	2.01	6.07	63
	10	2.52	8.68	71		10	2.37	6.18	64

To assess the role of the diode pump source for the development of microchip lasers based on Yb-doped gallium garnets, we compare the optical-to-optical efficiency η_{opt} for Yb:LuGG, Yb:YGG, Yb:CNGG and Yb:CLNGG lasers with $T_{\text{OC}} = 10\%$ (yielding the best laser output) for 932 nm ($w_p \sim 52 \mu\text{m}$) or 969 nm ($w_p \sim 100 \mu\text{m}$) pumping, Fig. 9. One can see that at low pump levels, the diode #1 is beneficial as it provides lower laser threshold and thus much higher η_{opt} . However, at high pump level due to the above mentioned thermal roll-over, the use of diode #2 corresponds to higher laser efficiencies and better potential for power scaling.

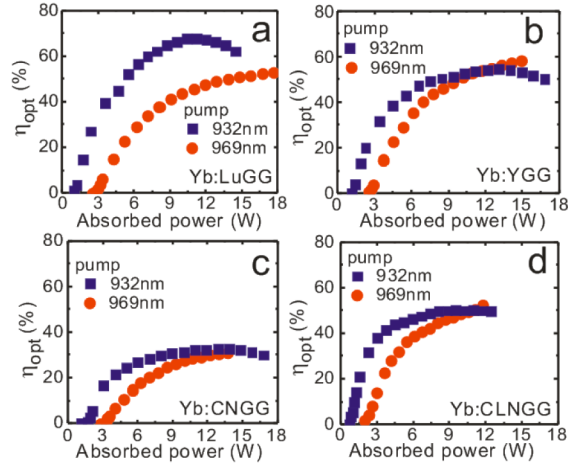


Fig. 9. Optical-to-optical efficiency η_{opt} for microchip lasers based on Yb:LuGG (a), Yb:YGG (b), Yb:CNGG (c) and Yb:CLNGG (d) crystals, $T_{\text{OC}} = 10\%$.

Table 4. Loss Coefficient for the Studied Crystals Estimated from the Caird Plot

Diode	δ, cm^{-1}			
	Yb:LuGG	Yb:YGG	Yb:CNGG	Yb:CLNGG
932 nm	0.0016	0.0026	0.0103	0.0118
969 nm	0.0012	0.0027	0.0141	0.0095

For CW microchip lasers, the intracavity losses are mainly linked to the active medium. To estimate them for the studied crystals, we utilized the method proposed by Caird et al. [29], i.e. we plotted the inverse of the slope efficiency vs. the inverse of the output coupling. This dependence is then expressed as $1/\eta = 1/\eta_0 + (L/\eta_0)1/T_{\text{OC}}$ where L is a round-trip internal loss and η_0 is an intrinsic slope efficiency. From the value of L and the crystal length (Table 1), we estimated the loss coefficient, δ . The results are presented in Table 4. For the loss calculations, we used the results obtained with the two diodes to increase the accuracy. For Yb:CNGG and Yb:CLNGG, the loss coefficient is at least three times higher than for Yb:LuGG and Yb:YGG. The higher loss is the main reason for the deterioration of the laser performance for the calcium gallium garnets.

To justify the correctness of the determined spectroscopic and thermo-optic properties of the studied crystals, as well as their loss characteristics, we have modeled the output performance of our lasers using a simple model of quasi-three level CW laser (without consideration of spatial and spectral distribution of the pump and laser fields). The following expressions for the laser threshold P_{th} and output power P_{out} were derived from the rate equations:

$$P_{\text{th}} = \frac{h\nu_p k_{\Sigma} + \sigma_{\text{abs}}^l N_{\text{Yb}}}{\tau_{\text{Yb}} \sigma_{\text{abs}}^l + \sigma_{\text{SE}}^l} l_{\text{act}} \pi w_p^2, \quad (2a)$$

$$P_{\text{out}} = \frac{w_l^2 k_{\text{OC}} \nu_p}{w_p^2 k_{\Sigma} \nu_l} (P_{\text{abs}} - P_{\text{th}}). \quad (2b)$$

Here, h is the Planck constant, ν_p and ν_l are the pump and laser frequencies, respectively, k_{Σ} is the total loss coefficient, $k_{\Sigma} = k_{\text{OC}} + k_{\text{loss}}$, where $k_{\text{OC}} = -\ln(1 - T_{\text{OC}})/2l_{\text{act}}$, l_{act} is the length of the active medium, the k_{loss} coefficient represents the passive losses, σ_{abs}^l and σ_{SE}^l are the absorption and SE cross-sections at the laser frequency ν_l , the term $\sigma_{\text{abs}}^l N_{\text{Yb}}$ stands for the reabsorption loss. Spectroscopic parameters of the crystals were taken in accordance with Fig. 3, pump and laser frequencies – with Fig. 1 and Fig. 6, characteristics of the laser elements –

with Table 1 and Table 4, and the radii of the laser mode w_l were calculated by using the thermal lens parameters presented in Fig. 4. The results of this modeling correlate well with the experimental data for all crystals, see Fig. 10 where experiment and modeling are presented for the particular cases of Yb:LuGG and Yb:CNGG. A profound deviation from the modeling (roll-over of the output dependence) is observed only when pumping with diode #1 at high pump levels, $P_{abs} > 12$ W. This is referred to significant heating of the crystal resulting in temperature-induced variation of spectroscopic and thermal properties of the material which is not considered in Eq. (2).

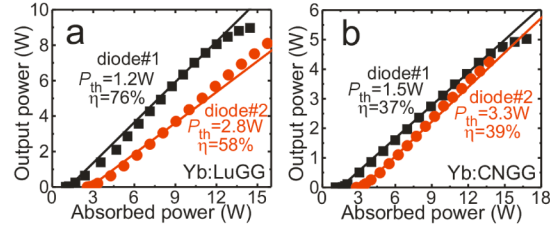


Fig. 10. Modeling of output performance of Yb:LuGG (a) and Yb:CNGG (b) lasers with Eq. (2), points – experimental data, lines are calculations; $T_{OC} = 10\%$. Numbers on the graph correspond to modeling.

All microchip lasers studied in the present work generated nearly circular output beams corresponding to the TEM_{00} mode with a Gaussian spatial profile. For 969 nm pumping, $M^2_{x,y}$ factors for the Yb:LuGG and Yb:YGG lasers were < 1.2 and for Yb:CNGG and Yb:CLNGG lasers, < 1.35 (at the highest pump level). For 932 nm pumping in the region of thermal roll-over, these values increased up to ~ 1.5 . The low ellipticity of the output beam is related to the low astigmatism of the thermal lens ($< 15\%$, as determined in the present paper) inherent to cubic crystals.

To evaluate the prospects of Ga garnets as hosts for Yb^{3+} ions, we have compared relevant spectroscopic and thermal figure-of-merits for these materials (Table 5).

Table 5. Comparison of Figure-of-Merits* for Yb-Doped Garnets**

Crystal***	$\lambda_{ZL} / \Delta\lambda$, nm	σ_{abs} , 10^{-20} cm^2	λ_{lum} , nm	σ_{SE} , 10^{-20} cm^2	τ_{Yb} , ms	κ , W/mK	η_h , %	χ/κ , 10^{-6} m/W
Yb:LuGG	970 / 1.8	2.7	1025	2.8	1.0 [6]	$\sim 5.8^{est.}$	5.4%	2.4
Yb:YGG	970 / 1.8	2.4	1025	2.6	1.1 [6]	$\sim 5.8^{est.}$	5.4%	2.3
Yb:CNGG	974 / 4.4	1.9	1028	1.9	0.8 [16]	$\sim 2.5^{est.}$	5.3%	5.9
Yb:CLNGG	972 / 3.5	2.6	1027	2.0	~ 0.7 [16]	$\sim 3.2^{est.}$	5.4%	4.5
Yb:YAG	968 / 2.8	0.8 [30]	1031 [30]	2.3 [30]	0.95 [30]	6.7 [4]	6.1%	2.2 [22]

* λ_{ZL} – wavelength of the zero phonon line in the absorption spectrum, $\Delta\lambda$ – FWHM of the absorption peak, λ_{lum} – main emission wavelength, σ_{SE} – stimulated-emission cross-section at λ_{lum} , τ_{Yb} – lifetime of Yb^{3+} ions, κ – thermal conductivity, $\eta_h = 1 - \lambda_{ZL}/\lambda_{lum}$ is the quantum defect, χ/κ is the thermal figure-of-merit, where χ is the “generalized” thermo-optic coefficient.

**Values without Ref. – this work.

***Crystal doping is specified in Table 1, for Yb:YAG it is 10 at.%.

As compared with Yb:YAG, all studied Ga garnets offer much stronger absorption at the zero-phonon line (i.e., for Yb:LuGG $\sigma_{abs} = 2.7 \times 10^{-20} \text{ cm}^2$ at 970 nm which is three times larger than for Yb:YAG, $\sigma_{abs} = 0.8 \times 10^{-20} \text{ cm}^2$ at 968 nm). This allows one to pump efficiently Yb-doped Ga garnets into this band thus reducing the heat loading in the crystal, as shown in the present work. Moreover, higher σ_{abs} value may allow for reduction of Yb doping level (which, in turn, will lead to a higher thermal conductivity). Among the Ga garnets, the disordered ones (CNGG and CLNGG) offer wider zero-phonon line (FWHM ~ 4 nm, compared with 1.8 nm for Yb:LuGG) which makes them less sensitive to the temperature drift of the diode wavelength. From the point of view of energy storage and generation of high pulse energies in the Q-switching operation mode, Yb-doped LuGG and YGG crystals

have higher potential due to longer lifetimes of Yb^{3+} ions, as compared with disordered Ga garnets and Yb:YAG.

If considering thermal properties, we can conclude that all Ga garnets are characterized by lower thermal conductivity κ as compared with Yb:YAG (at the same Yb doping level, 5...7 at.%). In terms of thermal figure-of-merit, χ/κ , where χ is the “generalized” thermo-optic coefficient, which is the characteristic parameter of thermo-optic effects being independent on the cavity configuration and pump spot size, the ordered Ga garnets show ($\chi/\kappa \sim 2.3 \times 10^{-6}$ m/W which is close to the value for Yb:YAG) and much better than for the disordered ones ($\chi/\kappa \sim 5...6 \times 10^{-6}$ m/W). In consequence, they are more suitable for laser configurations which require stable operation at high pump levels.

4. Conclusion

We report on a comparative study of thermal lensing and microchip laser performance of Yb-doped gallium garnets, Yb:YGG, Yb:LuGG, Yb:CNGG and Yb:CLNGG, diode-pumped at ~ 932 and 969 nm. It is shown that the thermal conductivity of all the studied Ga garnets is lower than that of Yb:YAG (at the same doping level of 5...7 at.%), however, Yb-doped Ga garnets offer much higher absorption cross-sections at the zero-phonon line at ~ 970 nm that allows efficient diode pumping into this band reducing the heat loading in the crystal. Strong zero-phonon line absorption, comparable thermo-optic behavior and longer lifetimes for Yb^{3+} ions for ordered Yb:REGG (RE = Y or Lu) crystals determine their potential usage in highly efficient microchip lasers generating higher pulse energies in the Q-switched mode (as compared with Yb:YAG). In the present work, output powers of ~ 9 W are generated at ~ 1.04 μm with CW Yb:REGG microchip lasers, slope efficiencies reaching 75% and an optical-to-optical efficiency of $\sim 63\%$. If comparing Yb:REGG crystals with disordered calcium Ga garnets, the latter suffer from poor thermo-optic properties and high internal losses (which can be reduced in future by appropriate growth conditions). Yb-doped disordered Ga garnets are however more interesting for mode-locked lasers as they offer broader emission bands.

Further work on microchip lasers based on Yb-doped gallium garnets will be focused on passive Q-switching by using, for instance, Cr^{4+} :YAG as a saturable absorber. As ordered Ga garnets exhibit the typically long radiative lifetime of the Yb^{3+} upper laser level ($^2\text{F}_{5/2}$), ~ 1.1 ms, this is favorable for high pulse energies. In addition, the microchip concept can provide very short (even, sub-ns) pulses [31] due to the reduced cavity round trip time.

Acknowledgments

This work was supported by the Spanish Government under projects, MAT2013-47395-C4-4-R and TEC2014-55948-R, and by the Generalitat de Catalunya under project 2014SGR1358. F.D. acknowledges additional support through the ICREA academia award 2010ICREA-02 for excellence in research. This work is part of a project that has received funding from the European Union’s Horizon 2020 research and innovation programme under the Marie Skłodowska-Curie grant agreement No 657630. This work is also supported by the European Regional Development Fund, the European Social Fund, and the state budget of the Czech Republic (Project HiLASE:CZ.1.05/2.1.00/01.0027) and by the Czech Science Foundation (GACR) under Project GA14-01660S.